# A simple analytical approach to simulate the electrochemical impedance response of flooded agglomerates in polymer fuel cells

A. Baricci *, A. Casalegno

*Politecnico di Milano, Department of Energy, Via Lambruschini 4, 20156 Milano, Italy*

Received 2 October 2014
Received in revised form 8 January 2015
Accepted 10 January 2015
Available online 13 January 2015

## 1. Introduction

The physics of polymer electrolyte fuel cell (PEMFC) cathode has been successfully represented by a set of differential equations based on the *pseudo* homogeneous continuum approximation [1,2]. The conventional approach consists in solving mass conservation equations across the catalyst layer (CL) for oxygen (Eq. (1)) and proton (Eq. (2)) along with phenomenological equations for closure, *e.g.* Ohm's law (Eq. (3)) and Fick's law of diffusion (Eq. (4)). The set of differential equations is reported for general catalyst layer 3D geometry:

$$\nabla\cdot\underline{j} = Q_H - C_{DL}\frac{\partial\eta}{\partial t} \tag{1}$$

$$\nabla\cdot\underline{\Phi}_O = Q_O - \frac{\varphi_{CL}}{RT}\cdot\frac{\partial p_{O2}}{\partial t} \tag{2}$$

$$\nabla\eta = -\frac{\underline{j}}{\sigma_{CL}} \tag{3}$$

$$\underline{\Phi}_O = -D_{CL}\frac{\nabla p_{O2}}{RT} \tag{4}$$

In which $\underline{j}$ is the local current density vector, $\underline{\Phi}_O$ is the local oxygen molar flux, $\eta$ is the overpotential of oxygen reduction reaction (ORR) and some properties of the CL are employed: the electrolyte conductivity ($\sigma_{CL}$), the double layer capacitance ($C_{DL}$), the effective diffusion coefficient of oxygen ($D_{CL}$), which accounts for molecular diffusion and Knudsen diffusion across CL secondary pores, and the secondary porosity ($\varphi_{CL}$) that is the volume of the void between agglomerates divided by total CL volume [3].

In addition to Eqs. (1)–(4), other phenomena have to be considered in the CL, *e.g.* water transport/flooding, that will either introduce additional equations or modify the reported ones.

Proton ($Q_H$) and oxygen ($Q_O$) sinks in Eqs. (1) and (2) are proportional to the volume averaged catalyst layer reaction rate, which is affected by sluggish mass transfer in the primary pores of the catalyst agglomerates that are partially/totally flooded by the electrolyte. Several approaches have been proposed to model the mass transport in the micro/meso pores of the catalyst layer agglomerates [3,4], but the most common alternatives are the macro-homogeneous model (MHM) and the flooded agglomerate model (FAM). While MHM neglects mass transport inside Platinum

* Corresponding author. Tel.: +39 02 2399 3840.
E-*mail address:* andrea.baricci@polimi.it (A. Baricci).

catalyst/Carbon support pellets where it postulates homogeneous concentration of reactants, FAM identifies an additional mass transport resistance inside the catalyst layer microstructure and for this reason is considered as the evolution of the MHM. Nevertheless, in the literature there is still debate regarding the validity of continuum based FAM [5], partially due to the difficulty in the estimation of the FAM parameters: agglomerate size and electrolyte fraction are generally calibrated on experimental polarization curves and as a consequence, microstructural parameters are roughly estimated, as reviewed by Dobson et al. [6]. Advanced *ex situ* experiments are a possible way to overcome this controversy, by directly estimating FAM parameters: recent works [7,8] adopted Nano-scale computed tomography imaging to estimate agglomerate relevant parameters.

An alternative and additional way to strengthen model validation [9] and to improve parameter estimation [10] deals with information provided by the electrochemical impedance spectroscopy (EIS). The development of physical based models of EIS has shown the potentiality to separate Ohm kinetic and mass transport polarizations with reasonable computational power, if any Fourier transform based solution method is used [9–14]. Unfortunately, when dealing with the impedance response of the agglomerate, a cumbersome analytical solution is obtained for simple 1D spherical [12] and planar [15] geometry and, as a consequence, no further development has been observed in research on this topic. The known alternative is the numerical integration of the agglomerate impedance response, as done by D. Gerteisen et al. [13], which increases significantly the simulation time.

The idea behind this work is to develop a new, fast and simple method that leads to an accurate analytical expression for the impedance response of FAM, regardless of the agglomerate geometry. During EIS, a small sinusoidal oscillation of potential is imposed over steady state and causes a small oscillation of the reaction rate. In turn, the local oxygen consumption and oxygen concentration in the flooded agglomerate oscillate. As hypothesis of FAM [12] the agglomerates are considered as totally flooded by the electrolyte and thus oxygen is dissolved in it. In the general case, the volume of dissolved oxygen within the agglomerate compensates for dynamical consumption, damps the oscillation and introduces a phase-shift between the sinusoidal oscillation of potential and the sinusoidal oscillation of agglomerate current. The presented approach is based on the observation that the volume of the agglomerate is quite small, in agreement with recent works [6], and dynamics of oxygen concentration are very fast and occur at high frequency. It is thus concluded that phase-shift or damping due to oxygen accumulated in the agglomerate is negligible at typical cathode charge transfer frequency. For this reason it has no visible effect on EIS because it occurs in a frequency range in which the double layer acts as a short circuit. The reported assumption, which validity is recognized to be wide and discussed in Section 3.1, significantly reduces the mathematical and numerical complexity of the impedance response. In the following sections, the theory of generalized FAM is discussed by creating an analogy between the steady state solution and the solution with superimposition of a small sinusoidal signal.

## 2. Theory

### *2.1. Generalized flooded agglomerate steady state or DC model equations*

The representation of the cathode of a PEMFC according to flooded agglomerate model is reported in Fig. 1. The catalyst layer is simplified as composed of two subdomains: the secondary macro pores that are responsible for oxygen transfer across the CL; the porous agglomerates where electrochemical reaction takes place.

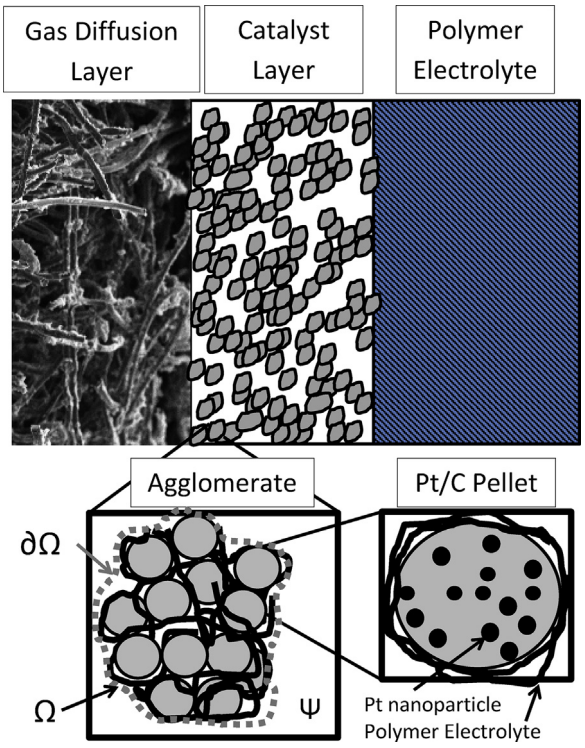


**Fig. 1.** Schematic illustration of the cathode of a PEMFC. Gas Diffusion Layer, Catalyst Layer and Polymer Electrolyte Membrane are highlighted. The agglomerate sub-domain composed of Platinum/Carbon pellets and polymer binder is shown in the bottom left zoom. Platinum/Carbon porous catalyst pellets are reported in the bottom right zoom. $\Omega$ is the agglomerate subdomain and $\partial\Omega$ the boundary between agglomerate and secondary pores/other agglomerates.

Accordingly with other works [12], primary porosity in the agglomerates is supposed to be totally flooded by the polymer electrolyte. W. K. Epting, and S. Litster [8] estimated that the void fraction in the agglomerate is low, approximately 0.10 and it is mostly composed of solid and polymer phases.

The generalized flooded agglomerate domain considered in this work is described below. The overall domain is indicated by $\Psi$ and is a three dimensional portion of the CL which is divided in two regions or subdomains. The agglomerate subdomain is indicated by $\Omega$ and is the volume containing the Pt/C catalyst pellets totally flooded by the electrolyte, *i.e.* Nafion, phosphoric acid or the proton conducting medium. The porous subdomain is the region of the CL where gas and/or liquid water are present. By definition, the porous region is indicated by $[\Psi - \Omega]$. The boundary between the agglomerate and porous subdomains or other agglomerates that are in proximity (indicated by $\partial\Omega$) is the frontier through which proton and oxygen are transferred to the active catalyst sites. According to the previous notation, the definition of CL porosity is:

$$\varphi_{CL} = \frac{\iiint_{\Psi-\Omega} dV}{\iiint_{\Psi} dV} \tag{5}$$

In the agglomerate subdomain four variables are defined: the scalar overpotential for ORR ($\eta$), the scalar concentration of dissolved oxygen in the electrolyte ($C$), the proton flux vector ($\underline{J_H}$) and the oxygen diffusive flux vector ($\underline{J_O}$). If the agglomerate length scale is significantly higher than the diffusion and catalyst nanoparticle length scales, continuum approximation is valid, thus proton conservation (Eq. (6)) and oxygen conservation (Eq. (7)) are:

$$\nabla \cdot \underline{J}_H^0 = 4Fr^0 \tag{6}$$

$$\nabla \cdot \underline{J}_O^0 = r^0 \tag{7}$$

According to A. A. Kulikovsky [14] the suffix 0 indicates a steady state variable. The local oxygen reaction rate ($r^0$) is modelled by means of the Tafel Law as generally done for ORR in PEMFC [12,15]:

$$r^0 = -\frac{i_*(1-\theta)}{4F}\left(\frac{C^0}{C_{ref}}\right)\exp\left(\frac{\eta^0}{b}\right) \tag{8}$$

Overpotential is taken positive for reduction and $\theta$ is the electrolyte fraction in the agglomerate. The closure of the equation system is obtained by means of two phenomenological equations describing the oxygen and the proton fluxes, the Ohm's Law (Eq. (9)) and the Fick's Law of diffusion (Eq. (10)):

$$\underline{J}_H^0 = -\sigma^* \nabla \eta^0 \tag{9}$$

$$\underline{J}_O^0 = -D^* \nabla C^0 \tag{10}$$

At the boundary $\partial\Omega$ Dirichlet condition is imposed, being the partial pressure of oxygen in the pore volume fixed by the CL problem and $H$ is a solubility coefficient:

$$C = Hp_{O2}^0 \Leftrightarrow \forall \underline{x} \in \partial\Omega \tag{11}$$

By introducing a problem related length scale (indicated by $R_{AGG}$ *e.g.* the agglomerate mean radius for spherical agglomerate geometry), non-dimensional variables are introduced:

$$\underline{\tilde{x}} = \frac{\underline{x}}{R_{AGG}}, \tilde{C} = \frac{C}{Hp_{O2}^0}, \underline{\tilde{J}}_H = \frac{\underline{J}_H R_{AGG}}{4FD^* Hp_{O2}^0}, \underline{\tilde{J}}_O = \frac{\underline{J}_O R_{AGG}}{D^* Hp_{O2}^0}, \tilde{\eta} = \frac{\eta}{b} \tag{12}$$

Ohm's Law (Eq. (9)) in non-dimensional form is reported in Eq. (13). A new non-dimensional parameter ($\xi$) is introduced, which definition is available in Eq. (14):

$$\underline{\tilde{J}}_H^0 = -\frac{\nabla \tilde{\eta}^0}{\xi} \tag{13}$$

$$\xi = \frac{p_{O2}^0 HD^*}{\sigma b} \tag{14}$$

If it is true that $\xi << 1$ the overpotential scalar field is homogeneous inside the agglomerate. Since the proton conductivity of the electrolyte phase in the agglomerate is high (in the order of 0.1–1 S cm$^{-1}$), the overpotential is considered homogeneous in the agglomerate region.

Non-dimensional dissolved oxygen concentration is obtained by solving Eq. (15) that is a combination of Eqs (7),(8) and (10) in non-dimensional form, according to Eq. (21) in [12]:

$$\tilde{\nabla} \cdot \tilde{\nabla} \tilde{C}^0 = \phi_n^2 \tilde{C}^0 \tag{15}$$

The parameter that appears in Eq. (15) is known as Thiele modulus (indicated by $\phi_n$ and represents the ratio between the surface reaction rate and the diffusion rate across the agglomerate:

$$\phi_n = R_{AGG}\sqrt{\frac{i_*(1-\theta)}{4FC_{ref}D^*}\exp\left(\frac{\eta^0}{b}\right)} \tag{16}$$

According to FAM approach, the proton ($Q_H$) and oxygen ($Q_O$) sinks in the CL Eqs. (1) and (2) are the surface integral of proton and oxygen fluxes exchanged across the boundary between the porous region and the agglomerate domain, divided by the CL volume:

$$Q_{H/O}^0 = \frac{\iint_{\partial\Omega} \underline{\tilde{J}}_{H/O}^0 \cdot \hat{n} dS}{\iiint_\Psi dV} = \frac{\iiint_\Omega \left(\nabla \cdot \underline{\tilde{J}}_{H/O}^0\right) dV}{\iiint_\Psi dV} \tag{17}$$

In steady state, by means of the divergence theorem it is possible to prove that $Q^0$ is the volume averaged reaction rate of the CL and in non-dimensional form $\tilde{Q}_H^0 = \tilde{Q}_O^0$

There is a noteworthy limiting case of homogeneous concentration in the agglomerate domain, which is the trivial solution to Eq. (15) with condition $\phi_n^2 \ll 1$:

$$^*\tilde{C}^0 = 1 \Leftrightarrow \forall \underline{x} \in \Omega \tag{18}$$

As a consequence, whenever the surface reaction rate is the limiting phenomenon compared to the diffusion rate across the agglomerate, the FAM and the MHM become equivalent. In this special case, the volume averaged non-dimensional reaction rate is:

$$^*\tilde{Q}^0 = -\phi_n^2(1-\varphi_{CL}) \tag{19}$$

According to the classical approach, the link between the CL and the agglomerate problems is achieved by defining the effectiveness factor ($\varepsilon^0$) a non-dimensional parameter that represents the ratio of the volume averaged reaction rate in FAM to that in MHM:

$$\varepsilon^0 = \frac{\tilde{Q}^0}{^*\tilde{Q}^0} = \frac{\iiint_{\tilde{\Omega}} \tilde{C}^0 dV}{\iiint_{\tilde{\Omega}} dV} \tag{20}$$

According to its definition, the effectiveness factor is equal to 1 whenever $\phi_n^2 \ll 1$ and it is instead lower than 1 when the mass transport rate in the agglomerate domain determines a concentration gradient.

### *2.2. Generalized flooded agglomerate impedance or AC model equations*

Electrochemical impedance spectroscopy (EIS) is a frequency response measurement that consists in applying a small sinusoidal perturbation to the electrode potential in order to measure the frequency dependent impedance calculated as the ratio between the potential and the current sinusoidal signals. If the perturbation is adequately small, the system response is *pseudo* linear and each system property oscillates around the steady state at the same frequency of the imposed signal. From the mathematical point of view, the system variables are decomposed in the steady state or DC part and the perturbed or AC one.

Conservation and phenomenological equations discussed in Section 2.1 have to be extended to describe the transport of the AC variables in the agglomerate domain. The procedure that leads to the definition of the impedance problem consists in the following steps:

1 Conservation equations are written including the storage contribution or unsteady term, mathematically described by the time derivative.
2 Each variable is decomposed into the DC and the AC signal, *e.g.* a general variable ($f$) becomes $f = f^0 + f^1 e^{i\omega t}$ According to A. A. Kulikovsky [14] suffix 1 indicates the sinusoidal AC component of the signal at the angular frequency ω. The time derivative is computed as $\partial f/\partial t = i\omega f^1 e^{i\omega t}$.
3 The non-linear reaction rate is linearized around the steady state, with respect to overpotential $\eta$ and oxygen concentration (C):

$$r = r^0 + \left(dr^0/d\eta^0\right)\big|_C \eta^1 e^{i\omega t} + \left(dr^0/dC^0\right)\big|_\eta C^1 e^{i\omega t}. \tag{20}$$

4 The steady state equation simplifies and the result is a linear partial differential equation in which the time variable has been eliminated.

The reported procedure is applied to steady state proton conservation Eq. (6) to obtain the conservation equations for oscillating proton flux in the agglomerate domain:

$$\nabla\cdot\underline{J}_H^1 = r^0\left[\frac{C^1}{C^0} + \frac{\eta^1}{b}\right] - \frac{C_{DL}}{(1-\varphi_{CL})(1-\theta)} i\omega\eta^1 \tag{21}$$

In analogy with the steady state problem, Ohm's law predicts homogeneous oscillating overpotential in the agglomerate domain if $\xi << 1$ Section 2.1). Under this hypothesis, the double layer current is a constant offset in the solution of oscillating proton flux and it is thus incorporated directly in the catalyst layer equation, consistently with Eq. (1). After this consideration, the conservation equations for oscillating proton (Eq. (22)) and oxygen (Eq. (23)) fluxes are reported below in non-dimensional form:

$$\tilde{\nabla}\cdot\tilde{\underline{J}}_H^1 = -{\phi_n}^2\left(\tilde{C}^1 + \tilde{C}^0\tilde{\eta}^1\right) \tag{22}$$

$$\tilde{\nabla}\cdot\tilde{\underline{J}}_O^1 = -\phi_n^2(\tilde{C}^1 + \tilde{C}^0\tilde{\eta}^1) - i\tilde{\omega}\tilde{C}^1 \tag{23}$$

The definition of non-dimensional radiant frequency is reported in Eq. (24), according to non-dimensional references reported in Eq. (12):

$$\tilde{\omega} = \frac{\omega\theta{R_{AGG}}^2}{D^*} \tag{24}$$

The AC oxygen concentration scalar field is the solution to Eq. (25):

$$\tilde{\nabla}\cdot\tilde{\nabla}\tilde{C}^1 = \left(\phi_n^2 + i\tilde{\omega}\right)\tilde{C}^1 + \phi_n^2\tilde{C}^0\tilde{\eta}^1 \tag{25}$$

A Dirichlet boundary condition is applied at the frontier concerning oxygen oscillation:

$$\tilde{C}^1 = \frac{p_{O2}^1}{p_{O2}^0} \Leftrightarrow \forall \underline{x} \in \partial\Omega \tag{26}$$

To link CL and agglomerate problems, the oxygen and proton AC fluxes are integrated over the agglomerate boundary, to obtain the molar AC fluxes of proton/oxygen exchanged between porous and agglomerate subdomains, per unit of CL volume:

$$Q_{H/O}^1 = \frac{\iint_{\partial\Omega}\underline{J}_{H/O}^1\cdot\hat{n}dS}{\iiint_\Psi dV} = \frac{\iiint_\Omega(\nabla\cdot\underline{J}_{H/O}^1)dV}{\iiint_\Psi dV} \tag{27}$$

By comparison of Eqs. (22) and (23) it is observed that, at low non-dimensional radiant frequency:

$$\tilde{Q}_H^1 = \tilde{Q}_O^1 \Leftrightarrow \tilde{\omega} \ll 1 \tag{28}$$

A noteworthy limit is studied in analogy with steady state, the limiting case in which FAM and MHM become equivalent. It is possible to demonstrate that it happens if both $\phi_n^2 \ll 1$ and $\tilde{\omega} \ll 1$ conditions occur. In this special case, the AC concentration is homogeneous inside the agglomerate:

$${}^*\tilde{C}^1 = \frac{p_{O2}^1}{p_{O2}^0} \Leftrightarrow \forall \underline{x} \in \Omega$$

As a consequence, the oscillating sinks in the CL model equations become:

$${}^*\tilde{Q}^1 = -\phi_n^2(1-\varphi_{CL})\left[\frac{p_{O2}^1}{p_{O2}^0} + \tilde{\eta}^1\right] \tag{29}$$

The reactant's flux oscillation is thus due to two separate effects: the oscillation of potential and the oscillation of the oxygen partial pressure.

In agreement with the classical approach it is possible to define AC effectiveness factors as corrections to be applied to the MHM reaction rate in order to incorporate FAM. It is observed that any effectiveness factor would make sense only under the hypothesis $\tilde{\omega} \ll 1$ otherwise frequency dependent complex numbers would result. A tentative definition is proposed here, where two distinct AC effectiveness factors are proposed, each one function of the Thiele modulus only:

$$\varepsilon_p^1 = \frac{\tilde{Q}^1|_{\eta_1=0}}{{}^*\tilde{Q}^1|_{\eta_1=0}} = \frac{\iiint_{\tilde{\Omega}}\left[\tilde{C}^1|_{\eta_1=0}\right]dV}{\frac{p_{O2}^1}{p_{O2}^0}\iiint_{\tilde{\Omega}}dV} \tag{30}$$

$$\varepsilon_\eta^1 = \frac{\tilde{Q}^1|_{p_1=0}}{{}^*\tilde{Q}^1|_{p_1=0}} = \frac{\iiint_{\tilde{\Omega}}\left[\tilde{C}^1\big|_{p_1=0} + \tilde{C}^0\tilde{\eta}^1\right]dV}{\tilde{\eta}^1\iiint_{\tilde{\Omega}}dV} \tag{31}$$

The use of two distinct AC effectiveness factors mimics Eq. (29), so that the sink term in the CL model equations become (under the hypothesis $\tilde{\omega} \ll 1$ thus $\tilde{Q}_H^1 = \tilde{Q}_O^1$

$$\tilde{Q}^1 = -\phi_n^2(1-\varphi_{CL})\left[\varepsilon_p^1\frac{p_{O2}^1}{p_{O2}^0} + \varepsilon_n^1\tilde{\eta}^1\right] \tag{32}$$

The analogy between the AC and DC problems sets a link between AC and DC effectiveness factors, as proved in Appendix A:

$$\varepsilon_p^1 = \varepsilon^0 \tag{33}$$

$$\varepsilon_\eta^1 = \varepsilon^0 + \frac{d\varepsilon^0}{d\phi_n}\cdot\frac{\phi_n}{2} \tag{34}$$

Eqs. (33) and (34) impose a universal expression for the impedance response of the generalized FAM, which can be easily computed by knowing the steady state effectiveness factor only,

regardless of the geometry. Eqs. (33) and (34) represent an innovative approach, valid under the hypothesis $\tilde{\omega} \ll 1$ which validity is discussed in Section 3.1.

### 2.3. Simple 1D agglomerate geometry

The theory developed in Sections 2.1 and 2.2 is applied on 1D planar, cylindrical and spherical agglomerate geometry, considering the radial direction as the prevalent direction of diffusion. Diffusion equation for the oscillation of dissolved oxygen concentration becomes:

$$\frac{1}{\tilde{r}^n}\frac{d}{d\tilde{r}}\left(\tilde{r}^n\frac{d\tilde{C}^1}{d\tilde{r}}\right) = \left(\phi_n^2 + i\tilde{\omega}\right)\tilde{C}^1 + \phi_n^2\tilde{C}^0\tilde{\eta}^1 \tag{35}$$

Eq. (35) is valid for planar geometry with n = 0, cylindrical with n = 1 and spherical with n = 2. As additional boundary condition, the solution is required to have null derivative at the symmetric boundary. In Table 1 the analytical expression of DC and AC effectiveness factors are reported for simple 1D geometries.

### 2.4. 1D planar catalyst layer AC equations

The AC CL continuum equations in planar 1D geometry are obtained by applying the procedure described in Section 2.2 to Eqs. (1)–(4). The resulting equations are analogous to the one reported in the literature [14]:

$$\frac{dj^1}{dx} = 4FQ^1 - i\omega C_{DL}\eta^1 \tag{36}$$

$$\frac{d\Phi_O^1}{dx} = Q^1 - i\omega\varphi_{CL}\frac{p_{O2}^1}{RT} \tag{37}$$

$$\frac{d\eta^1}{dx} = -\frac{j^1}{\sigma_{CL}} \tag{38}$$

$$\frac{dp_{O2}^1}{dx} = -RT\frac{\Phi_O^1}{D_{CL}} \tag{39}$$

The AC sink in FAM, under the hypothesis $\tilde{\omega} \ll 1$ is:

$$Q^1 = \frac{Q^0}{\varepsilon^0}\left[\varepsilon_p^1\frac{p_{O2}^1}{p_{O2}^0} + \varepsilon_\eta^1\frac{\eta^1}{b}\right] \tag{40}$$

Where the volume averaged steady state reaction rate from MHM is:

**Table 1**
Analytical expression for DC and AC Effectiveness factors for 1D planar, cylindrical, spherical geometry.

| Geometry | DC Effectiveness Factor $\varepsilon^0$/ AC Effectiveness Factor $\varepsilon^1{}_p$ | AC Effectiveness Factor $\varepsilon^1{}_\eta$ |
|---|---|---|
| 1D Planar | $\frac{\tanh(\phi_n)}{\phi_n}$ | $\frac{1}{2}[1 + \varepsilon^0 - (\phi_n\cdot\varepsilon^0)^2]$ |
| 1D Cylindrical | $\frac{2}{\phi}\cdot\frac{\mathrm{II}_1(\phi_n)}{\mathrm{II}_0(\phi_n)}$ | $\frac{1}{4}[4 - (\phi_n\cdot\varepsilon^0)^2]$ |
| 1D Spherical | $\frac{3}{\phi_n^2}[\phi_n\coth(\phi_n - 1)]$ | $\frac{1}{6}[9 - 3\varepsilon^0 - (\phi_n\cdot\varepsilon^0)^2]$ |

$$Q^0 = -\frac{i_*(1-\theta)(1-\varphi_{CL})}{4F}\left(\frac{Hp_{O2}^0}{C_{ref}}\right)exp\left(\frac{\eta^0}{b}\right)\varepsilon^0 \tag{41}$$

The CL problem is completed by the expression for the DC and AC effectiveness factors reported in Table 1 (Section 2.3).

Common boundary conditions for fuel cell problems, as reported and discussed in [14], at the membrane/CL interface (Eq. (42)) and at the GDL/CL interface (Eqs. (43)–(45)) are:

$$\Phi_O^1(x = 0) = 0 \tag{42}$$

$$j^1(x = \delta_{CL}) = 0 \tag{43}$$

$$\eta^1(x = \delta_{CL}) = \eta_1^1 \tag{44}$$

$$p_{O2}^1(x = \delta_{CL}) = 0 \tag{45}$$

Arbitrary oscillating overpotential is imposed at GDL/CL interface. Catalyst layer impedance is computed according to [14] as:

$$Z = \frac{\eta^1(x = 0)}{j^1(x = 0)} \tag{46}$$

## 3. Results and discussion

### 3.1. Validity of the hypothesis $\tilde{\omega} \ll 1$

The AC flooded agglomerate theory reported in Section 2.2 is applied to monodimensional planar, cylindrical and spherical geometry to discuss the validity of the underlying hypothesis and the meaning of the AC effectiveness factors introduced in Eqs. (33) and (34). The analysis focuses on the AC proton sink in the CL model ($Q_H^1$), which expresses the oscillating proton flux exchanged across the agglomerate boundary between the porous subdomain and the agglomerate subdomain. To enhance clarity in plot and avoid large scale variation associated to large variation in Thiele Modulus, a new parameter is introduced:

$$\lambda_H^1 = \frac{\tilde{Q}_H^1}{{}^*\tilde{Q}_H^1} \tag{47}$$

That is defined as the AC proton sink in FAM divided by the AC proton sink in MHM.

In Fig. 2 and 3 the real part of the non-dimensional parameter $\lambda_H^1$ is computed numerically and plotted as a function of the non-dimensional angular frequency for planar, cylindrical and spherical geometry. The low Thiele modulus condition is not reported: it is observed from the definition that when Thiele modulus becomes small, $\lambda_H^1$ tends to 1. In Fig. 2 the analysis focuses on the case $p_{O2}^1 = 0$ while in Fig. 3 the case $\eta^1 = 0$ is reported for completeness. In both plots it is evident that at low frequency $\lambda_H^1$ becomes equal to the AC effectiveness factor and the validity of Eqs. (33) and (34) is verified in the tested cases. In addition, it is deduced from Figs. 2 and 3 that the low frequency limit is reasonably reached at any frequency lower than $f_0 = D^*/(2\pi\theta {R_{AGG}}^2)$ *i.e.* $\tilde{\omega} < 1$, regardless of the considered geometry. At high Thiele modulus ($\phi_n > 1$) the low frequency limit is reached at higher frequency (10 or even 100 $f_0$). A quick look at Eq. (24) suggests that the low frequency limit could be reached approximately if $\tilde{\omega} < \left(\phi_n^2\varepsilon^0\right)$, but in the rest of

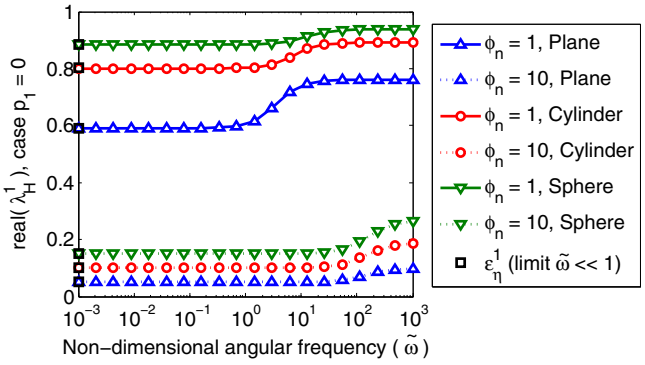


**Fig. 2.** Real part of the AC proton sink from FAM divided by the AC proton sink from MHM in the case $\eta^1 = 0$. Thiele modulus: 1 (continuous line) and 10 (dotted line) for 1D planar, cylindrical and spherical geometry. The squares indicate the AC effectiveness factor from Eq. (34).

the manuscript it is referred to the condition $\tilde{\omega} < 1$ for simplicity. Same conclusions are drawn by the analysis of the oxygen sink in the CL equations, which is not reported for conciseness.

The $\tilde{\omega} < 1$ condition requires that oxygen dissolved within the agglomerate does not damp the impedance response and the oscillation of the agglomerate current response is in phase with the oscillation of potential. From a physical point of view, the small flooded domain has a very fast response time, so that the agglomerate transient vanishes in a very short characteristic time. In the frequency domain, the agglomerate characteristic frequency is high if compared to cathode charge transfer frequency range.

To prove the validity of the hypothesis in PEM models, in Table 2 agglomerate characteristic frequency $f_0$ is reported for PEMFC, PAFC and HT-PEMFC agglomerate data from the literature [6,12,13,16–23]. If the agglomerate radius is lower than 500 nm, $f_0$ is in the order of 1 kHz–1 MHz, thus higher than cathode charge transfer typical frequency range (10–100 Hz). When the agglomerate radius is in the micron scale, $f_0$ is lower than 1 kHz and in one case it overlaps with the cathode kinetic feature in the spectrum [12]. This is due to the combination of high agglomerate radius and low diffusivity of oxygen in the electrolyte. It is important to evidence that more recent experimental works agree in setting a proper agglomerate length scale in the order of 100 nm [6] in comparison with older works because of technological update. The case $\tilde{\omega} > 1$ will be considered in Section 3.3.

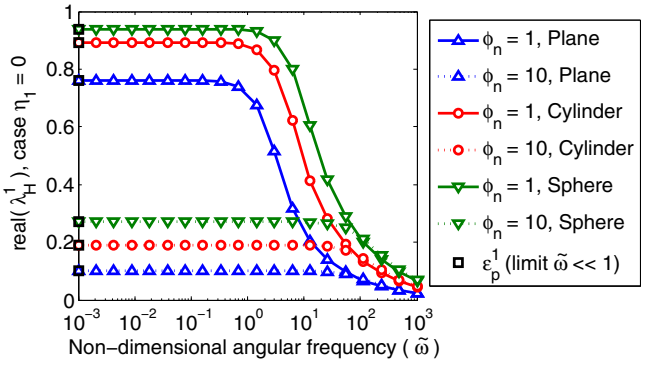


**Fig. 3.** Real part of the AC proton sink from FAM divided by the AC proton sink from MHM in the case $p_{02}^1 = 0$. Thiele modulus: 1 (continuous line) and 10 (dotted line) for 1D planar, cylindrical and spherical geometry. The squares indicate the AC effectiveness factor from Eq. (33).

### 3.2. Simulation of the CL impedance

To deepen the understanding of the AC effectiveness factors, the 1D planar CL model equations derived in Section 2.4 have been integrated to show the effect of the FAM on the impedance response. Input parameters, referring to a cathode of a PEMFC, are reported in Table 3 for spherical agglomerate geometry [6].

The limiting case of a thin layer electrode with homogeneous oxygen concentration and homogeneous overpotential across the catalyst layer is first considered. In Fig. 4, simulations of the impedance response of the catalyst layer are reported in the Nyquist plane for Thiele modulus ranging from 0.1 to 100. In the same plot a comparison is performed between the full agglomerate model [12] and the simplified model assuming $\tilde{\omega} < 1$. It is evident that the new approach developed in this work is adequate to represent the impedance of FAM, since the spectra computed with the full model and the simplified model overlap. The analysis of Fig. 4 leads to some conclusions regarding the impedance response of FAM: the spectrum of a thin layer electrode in the Nyquist plane is described by a capacitive circular feature, which diameter is widely defined as the charge transfer resistance. If FAM contribution is negligible, the charge transfer resistance of thin layer electrode is a well-known function of average current density ($j_0$): $R_{CT,TL} = b/j_0$. As observed in Fig. 4, at low Thiele modulus (or low current density) FAM predicts the charge transfer resistance of thin layer model, while at high Thiele modulus (or high current density) FAM charge transfer resistance is higher than $R_{CT,TL}$ until the apparent doubling of the Tafel slope is observed.

In a thin layer electrode with FAM, a simple integration of the catalyst layer equations (Section 2.4) leads to the following analytical expression for the charge transfer resistance:

$$R_{CT,FAM} = \frac{b}{j_0}\frac{\varepsilon^0}{\varepsilon_\eta^1} \tag{48}$$

It is expected from the apparent doubling of the Tafel slope that:

$$\lim_{\phi_n \to \infty} \frac{R_{CT,FAM}}{R_{CT,TL}} = \lim_{\phi_n \to \infty} \frac{\varepsilon^0}{\varepsilon_\eta^1} = 2 \tag{49}$$

Consequently AC effectiveness factor could be intended as a correction coefficient to the charge transfer resistance to account for the sluggish oxygen transport in the agglomerate. The deviation of FAM from MHM consists thus in the increase of the charge transfer resistance at high current density in comparison to the one estimated by MHM.

In Fig. 5 the AC effectiveness factors are plotted as a function of the Thiele Modulus for three geometries. While increasing the

**Table 2**
Calculation of agglomerate characteristic frequency with data from literature.

| Reference | D* (x10$^6$) cm$^2$ s$^{-1}$ | $R_{AGG}$ nm | θ – | $f_0$ Hz | Year |
|---|---|---|---|---|---|
| Cetinbas [22] | 3.1 | 1000 | 0.5 | $1{\cdot}10^2$ | 2014 |
| Marquis [16] | 45.0 | 150 | 0.66 | $5{\cdot}10^4$ | 2013 |
| Dobson [6] | 0.7 | 190 | 0.17 | $2{\cdot}10^3$ | 2012 |
| Kamarayugadda [23] | 1 | 200 ÷ 1000 | 0.4 | $4{\cdot}10^1 \div 10^3$ | 2012 |
| Yoon [19] | 85.0 | 100 | 0.5[a] | $3{\cdot}10^5$ | 2011 |
| Sousa [21] | 3.50 | 500 | 0.3 | $7{\cdot}10^2$ | 2010 |
| Gerteisen [20] | 0.50 | 200 | 0.4 | $5{\cdot}10^2$ | 2009 |
| Gerteisen [13] | 20.0 | 100 | 0.5[a] | $6{\cdot}10^3$ | 2007 |
| Choudhury [17] | 100.0 | 1000 | 0.5[a] | $3{\cdot}10^3$ | 2006 |
| Shah [18] | 0.8 | 200 | 0.2 | $2{\cdot}10^3$ | 2006 |
| Guo [12] | 2.2 | 1000 | 0.5 | $7{\cdot}10^1$ | 2004 |

[a] estimated because not reported in reference.

**Table 3**
PEMFC parameters adopted in the simulations of the CL impedance.

| Parameter | Value |
|---|---|
| T/C | 80 |
| θ | 0.17 |
| H/mol cm$^{-3}$ Pa$^{-1}$ | $3.16{\cdot}10^{-11}$ |
| $R_{AGG}$/nm | 190 |
| b/mV | 40 |
| i*/A cm$^{-3}$ | $9.3{\cdot}10^{-3}$ |
| D*/cm$^2$ s$^{-1}$ | $0.7{\cdot}10^{-7}$ |
| $\delta_{CL}$/μm | 10.0 |
| $C_{DL}$/F cm$^{-3}$ | 40 |
| $\varphi_{CL}$ | 0.30 |

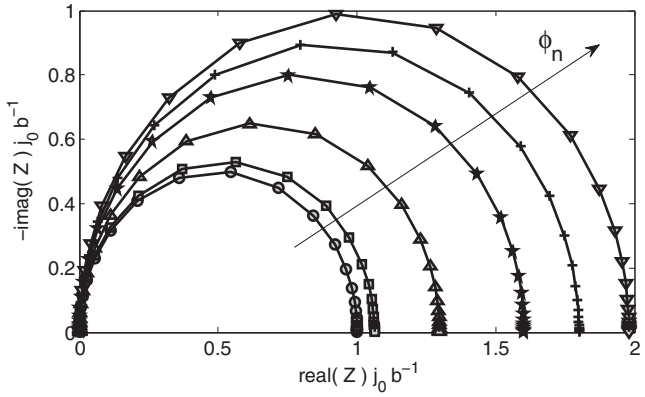


**Fig. 4.** Nyquist plot of catalyst layer impedance of thin layer electrode at different values of Thiele Modulus: 0.1 (O), 1 (□), 2.5 (△), 5 (☆), 10 (+), 100 (▽). Continuous line is used for the simulations with the innovative approach (Eqs. (33) and (34)).

Thiele modulus, the AC effectiveness factors decrease from a value of 1 with a very fast decrease around $\phi_n = 1$, consistently with what already known regarding the steady state effectiveness factor. Differences between considered geometries become evident, since higher catalyst utilization is obtained in the spherical geometry. Planar and cylindrical agglomerates show higher charge transfer resistance than spherical ones, if the same agglomerate properties are obtained.

In analogy with [2], the impedance response with ideal oxygen transport across the CL (Supplementary Material 1) and ideal ionic transport across the CL (Supplementary Material 2) are numerically investigated. In both cases an apparent increase of the Tafel slope up to a factor of 4 could be observed on a theoretical basis.

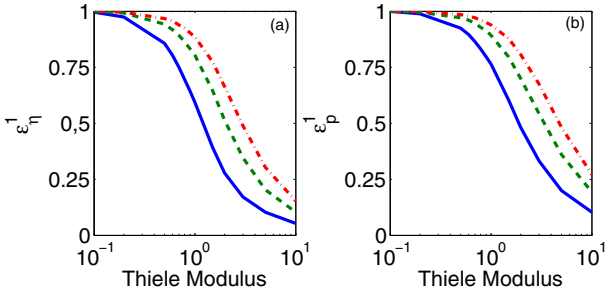


**Fig. 5.** AC effectiveness factors plotted as a function of Thiele Modulus. (a) case $p^1_{O2} = 0(\varepsilon^1_\eta)$; (b) case $\eta^1 = 0(\varepsilon^1_p)$. Planar (−), cylindrical (-) and spherical geometry (.-).

### 3.3. The investigation of the validity of the new approach: the case $\tilde{\omega} > 1$

Simulations considering $\tilde{\omega} > 1$ are reported in Fig. 6 and obtained by artificially shifting the charge transfer feature at higher frequency (from $10^3$ to$10^6$ Hz) by progressively decreasing the double layer capacitance. If $\tilde{\omega} > 1$ the approach developed in this work fails in correctly reproducing the imaginary part of the spectrum, but it still succeeds in simulating the low frequency resistance. As expected the deviation is more evident at high $\tilde{\omega}$ being still acceptable if $\tilde{\omega} < 10$. The oscillation of oxygen inside the agglomerate results in a distortion of the imaginary part which is not reproduced in the simplified model. In a limiting case of very low double layer capacitance (not physical for PEM cathode), FAM will generate a separate feature at lower frequency. The approach discussed here has thus been proved to be effective in reproducing the charge transfer resistance even when the underlying hypothesis is not verified.

### 3.4. Application of catalyst layer model to experimental data

Theoretical work described in the previous sections has been applied to experimental EIS recorded on a high temperature PEM fuel cell based on phosphoric acid polybenzimidazole membrane [9]. The use of a high temperature PEMFC allows neglecting the effect of water flooding because of operating temperature higher than boiling point of water. Experiments have been carried out at high oxygen stoichiometry (10) to guarantee uniform concentration in the distributors and avoid the presence of low frequency/channel features on EIS [24]. The use of high oxygen molar fraction (>50%) allows minimizing the effect of mass transport resistance in the gas phase due to GDL. Additional information concerning experimental setup, procedures and MEA samples is available in [9].

In Fig. 7, experimental impedance spectra of cathode catalyst layer recorded at 1.0 A cm$^{-2}$ are presented for oxygen molar fractions of 100%, 80% and 50%. By lowering the oxygen concentration the ORR overpotential increases and, consequently from Eq. (16), Thiele Modulus increases. The reported spectra are interpreted by means of the CL model presented in Section 2.4 with values of model parameters reported in Table 4. Additional modelling of the GDL according to [9] has been introduced. The agglomerate radius is estimated by model calibration and the reported value is reasonably in agreement with other works [6]. FAM is also reported to provide a better fit to experimental data if compared to MHM in the specific case of interest.

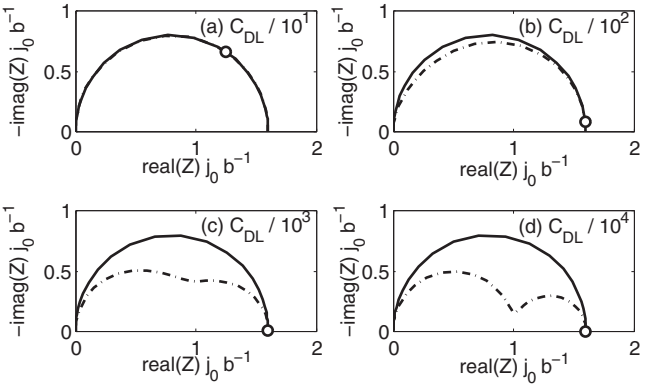


**Fig. 6.** Impedance spectra simulated with the new approach (continuous line) and the exact solution (dashed line) for different values of double layer capacitance. The circles indicate the position in the spectrum where the condition $\tilde{\omega} = 1$ occurs ($f$=2 kHz). Thiele modulus: 5.

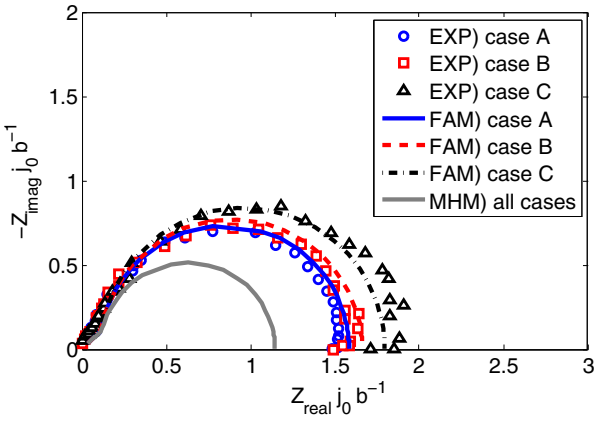


**Fig. 7.** Comparison between experimental and simulated EIS of high temperature PEMFC cathode. Temperature 160 °C, oxidant stoichiometry 10, dry reactants, current density 1.0 A cm$^{-2}$. Inlet oxygen molar fraction: case A) 100%, case B) 80%, case C) 50%. By decreasing oxygen concentration Thiele modulus increases and agglomerate size can be fitted.

**Table 4**
HT-PEMFC parameters adopted in the simulations.

| Parameter | Value | Reference |
|---|---|---|
| $\theta$ | 0.20 | [21] |
| H/mol cm$^{-3}$ Pa$^{-1}$ | $1.2{\cdot}10^{-12}$ | [21] |
| $R_{AGG}$/nm | 270 | Calibrated |
| b/mV | 51 | [21] |
| i* $(4FC_{ref})^{-1}$/s$^{-1}$ | 0.996 | Calibrated |
| D*/cm$^2$ s$^{-1}$ | $3{\cdot}10^{-6}$ | [21] |
| $D_{GDL}$/cm$^2$ s$^{-1}$ | 0.05 | Measured |
| $\delta_{GDL}$/μm | 200 | Measured |
| $D_{CL}$/cm$^2$ s$^{-1}$ | 0.02 | Measured |
| $\sigma_{CL}$/S cm$^{-1}$ | 0.10 | Calibrated |
| $\delta_{CL}$/μm | 18 | Measured |
| $C_{DL}$/F cm$^{-3}$ | 30 | Calibrated |
| $\varphi_{CL}$ | 0.50 | Assumed |

## 4. Conclusions

A new approach has been proposed in this work to compute the impedance response of the flooded agglomerate model. In analogy with the steady state analysis, AC effectiveness factors have been defined to create a link between agglomerate and CL equations. The analysis demonstrates that the AC effectiveness factors are corrective coefficients to the cathode feature in EIS: the sluggish oxygen transport in the agglomerates is responsible for increasing the cathode charge transfer resistance.

The definition of AC effectiveness factors has been restricted to the case when $f < D^*/(2\pi\theta {R_{AGG}}^2)$ but virtually all of the existing agglomerate models fall into this category. If this hypothesis is not valid, the presented approach fails in correctly reproducing the distortion in the imaginary part of the spectrum due to FAM, but it is still capable of simulating the low frequency resistance.

A significant improvement has been achieved by proving that the AC effectiveness factors are linked to the steady state effectiveness factor, according to Eqs. (33) and (34). If compared to the analytical solutions reported in the literature [12,15] a significant reduction in complexity and increase in generality has been achieved. This new approach opens the door to a new generation of analytical solutions of the FAM impedance response, *e.g.* with thin film diffusion or improved geometry.

Thanks to the new approach, it is possible to incorporate FAM in MHM with analytical like computational cost and significant improvement of existing models is expected. The application of the theoretical considerations original in this work to experimental EIS, as reported in Section 3.4, supports the validity of FAM for modelling of mass transport in the cathode catalyst layer microstructure and finds in EIS and powerful tool to improve PEMFC modelling. It is concluded that physical based modelling of EIS could be widely employed in the next years in addition to modelling of polarization curve.

## APPENDIX A

In the limit $\tilde{\omega} \ll 1$ the non-dimensional AC oxygen concentration in the electrolyte is the solution to the differential equation:

$$\tilde{\nabla} \cdot \tilde{\nabla}\tilde{C}^1 = \phi_n^2 \tilde{C}^1 + \phi_n^2 \tilde{C}^0 \tilde{\eta}^1 \qquad \text{A.1}$$

A Dirichlet boundary condition is applied on the frontier concerning oxygen oscillation:

$$\tilde{C}^1 = \frac{p_{O2}^1}{p_{O2}^0} \Leftrightarrow \forall \underline{x} \in \partial\Omega \qquad \text{A.2}$$

Solution to linear Eq. A.1 in the general case is achieved separating the superimposed problems of overpotential and oxygen pressure oscillation:

$$\tilde{C}^1 = \tilde{C}^1|_{\tilde{\eta}^1=0} + \tilde{C}^1|_{p^1=0} \qquad \text{A.3}$$

When $\tilde{\eta}^1 = 0$ the Eq. A.1 becomes totally equivalent to the steady state Eq. (15), with different boundary value:

$$\tilde{C}^1|_{\tilde{\eta}^1=0} = \tilde{C}^0 \frac{p_{O2}^1}{p_{O2}^0} \Leftrightarrow \tilde{\omega} \ll 1 \qquad \text{A.4}$$

When $p_{O2}^1 = 0$ the solution of Eq. A.1 is verified to be:

$$\tilde{C}^1|_{p^1=0} = \frac{d\tilde{C}^0}{d\tilde{\eta}^0}\tilde{\eta}^1 \qquad \text{A.5}$$

To verify the validity of Eq. A.5 it is substituted into Eq. A.1:

$$\tilde{\nabla} \cdot \tilde{\nabla} \left( \frac{d\tilde{C}^0}{d\tilde{\eta}^0} \right) \triangleq \phi_n^2 \frac{d\tilde{C}^0}{d\tilde{\eta}^0} + \phi_n^2 \tilde{C}^0 \qquad \text{A.6}$$

On the left hand side the derivative with respect to overpotential can be taken out of the La Place operator since the overpotential is not a space variable in the agglomerate subdomain. On the right hand side a derivative of a product is recognized, since $d(\phi_n^2)/d\tilde{\eta}^0 = \phi_n^2$ :

$$\phi_n^2 d\frac{\tilde{C}^0}{d\tilde{\eta}^0} + \phi_n^2 \tilde{C}^0 = \frac{d\left(\phi_n^2 \tilde{C}^0\right)}{d\tilde{\eta}^0} \qquad \text{A.7}$$

In conclusion, the validity of Eq. A.5 as the solution to Eq. A.1 (in the specific case is verified:$p_{O2}^1 = 0$

$$\frac{d}{d\phi_n}\left(\tilde{\nabla} \cdot \tilde{\nabla}\tilde{C}^0 - \phi_n^2 \cdot \tilde{C}^0\right) \triangleq 0 \qquad \text{A.8}$$

The final step consists in substituting the solution of the AC oxygen concentration into the AC effectiveness factors' definitions (Eqs. (30) and (31)) to prove Eqs. (33) and (34).

$$\varepsilon_p^1 = \frac{\iiint_{\tilde{\Omega}} \left[\tilde{C}^0\right] dV}{\iiint_{\tilde{\Omega}} dV} = \varepsilon^0$$

$$\varepsilon_\eta^1 = \frac{\int\int\int_{\tilde{\Omega}} \left[\frac{d\tilde{C}^0}{d\phi_n} \cdot \frac{\phi_n}{2} + \tilde{C}^0\right] dV}{\int\int\int_{\tilde{\Omega}} dV} = \frac{d\varepsilon^0}{d\phi_n}\frac{\phi_n}{2} + \varepsilon^0 \qquad \text{A.10}$$

An alternative way to prove the validity of Eqs. (33) and (34) consists in obtaining the AC volume averaged reaction rate by linearizing directly the steady state volume average reaction rate:

$$Q = Q^0 + (dQ^0/d\eta^0)|_c \eta^1 e^{i\omega t} + (dQ^0/dC^0)|_\eta C^1 e^{i\omega t}$$

Keeping in mind that the steady effectiveness factor is a function of the steady overpotential $\varepsilon^0 = \varepsilon^0(\eta^0)$, Eqs. (33) and (34) can be individuated after performing the derivative.

## Appendix A. Supplementary data

Supplementary data associated with this article can be found, in the online.

## References


[1] D.M. Bernardi, M.W. Verbrugge, A mathematical model of the solid-polymer-electrolyte fuel cell, J. Electrochem. Soc. 139 (1992) 2477.

[2] A.A. Kulikovsky, The regimes of catalyst layer operation in a fuel cell, Electrochim. Acta 55 (2010) 6391.

[3] M. El Hannach, T. Soboleva, K. Malek, A.A. Franco, M. Prat, J. Pauchet, S. Holdcroft, Characterization of pore network structure in catalyst layers of polymer electrolyte fuel cells, J. Power Sources 247 (2014) 322.

[4] Q. Wang, D. Song, T. Navessin, S. Holdcroft, Z. Liu, A mathematical model and optimization of the cathode catalyst layer structure in PEM fuel cells, Electrochim. Acta 50 (2004) 725.

[5] A.A. Kulikovsky, How important is oxygen transport in agglomerates in a PEM fuel cell catalyst layer? Electrochim. Acta 130 (2014) 826.

[6] P. Dobson, C. Lei, T. Navessin, M. Secanell, Characterization of the PEM fuel cell catalyst layer microstructure by nonlinear least-squares parameter estimation, J. Electrochem. Soc. 159 (2012) B514.

[7] S. Litster, W.K. Epting, E.A. Wargo, S.R. Kalidindi, E.C. Kumbur, Morphological analyses of polymer electrolyte fuel cell electrodes with nano-scale computed tomography imaging, Fuel Cells 13 (2013) 935.

[8] W.K. Epting, S. Litster, Effects of an agglomerate size distribution on the PEFC agglomerate model, Int. J. Hydrogen Energy 37 (2012) 8505.

[9] A. Baricci, M. Zago, A. Casalegno, A quasi 2d model of a high temperature polymer fuel cell for the interpretation of impedance spectra, Fuel Cells 14 (2014) 926.

[10] A.A.Kulikovsky,M.Eikerling,Analyticalsolutionsforimpedanceofthe cathode catalystlayerinPEMfuelcell:layerparametersfromimpedance spectrum withoutfitting,J.Electroanal.Chem.691(2013)13.

[11] T.E. Springer, T.A. Zawodzinski, M.S. Wilson, S. Gottesfeld, Characterization of polymer electrolyte fuel cells using AC impedance spectroscopy, J. Electrochem. Soc. 143 (1996) 587.

[12] Q. Guo, R.E. White, A steady-state impedance model for a PEMFC cathode, J. Electrochem. Soc. 151 (2004) E133.

[13] D. Gerteisen, A. Hakenjos, J.O. Schumacher, AC impedance modelling study on porous electrodes of proton exchange membrane fuel cells using an agglomerate model, J. Power Sources 173 (2007) 346.

[14] A.A. Kulikovsky, A physical model for catalyst layer impedance, J. Electroanal. Chem. 669 (2012) 28.

[15] T.E.Springer,I.D.Raistrick,Electricalimpedanceofaporewallfortheflooded-agglomeratemodelofporousgas-diffusionelectrodes,J.Electrochem.Soc.136 (1989)1594.

[16] J. Marquis, M.-O. Coppens, Achieving ultra-high platinum utilization via optimization of PEM fuel cell cathode catalyst layer microstructure, Chem. Eng. Sci. 102 (2013) 151.

[17] S.R. Choudhury, S.R. Choudhury, J. Rangarajan, R. Rengaswamy, Step response analysis of phosphoric acid fuel cell (PAFC) cathode through a transient model, Power Sources 140 (2005) 274.

[18] A.A. Shah, G.-S. Kim, W. Gervais, A. Young, K. Promislow, J. Li, S. Ye, The effects of water and microstructure on the performance of polymer electrolyte fuel cells, J. Power Sources 160 (2006) 1251.

[19] W. Yoon, A.Z. Weber, Modeling low-platinum-loading effects in fuel-cell catalyst layers, J. Electrochem. Soc. 158 (2011) B1007.

[20] D.Gerteisen,T.Heilmann,C.Ziegler,Modelingthephenomenaofdehydration and floodingofapolymerelectrolytemembranefuelcell,J.PowerSources187(2009) 165.

[21] T. Sousa, M. Mamlouk, K. Scott, An isothermal model of a laboratory intermediate temperature fuel cell using PBI doped phosphoric acid membranes, Chem. Eng. Sci. 65 (2010) 2513.

[22] F.C.Cetinbas,S.G.Advani,A.K.Prasad,Threedimensionalprotonexchange membranefuelcellcathodemodelusingamodifiedagglomerateapproach based ondiscretecatalystparticles,J.PowerSources250(2014)110.

[23] S.Kamarajugadda,S.Mazumder,Generalizedfloodedagglomeratemodelfor the cathodecatalystlayerofapolymerelectrolytemembranefuelcell,J.Power Sources208(2012)328.

[24] I.A. Schneider, S.A. Freunberger, D. Kramer, A. Wokaun, G.G. Scherer, Oscillations in gas channels: Part I. The forgotten player in impedance spectroscopy in PEFCs, J. Electrochem. Soc. 154 (2007) B383.